Optical Pumping and Magnetic Resonance

Dongwon Han and Kevin Wood
Stony Brook University
(Dated: March 13, 2017)

Optically pumped Rubidium (Rb) exposes its hyperfine structure at the neV energy scale by exhibiting stimulated emission from an alternating magnetic field at the corresponding frequency. Tracking the Zeeman energy splitting under the influence of various magnetic fields shows the magnetic moments of the ^{85}Rb and ^{87}Rb isotopes to be $\mu_{85} = (1.876 \pm 0.001) \times 10^{-5} \frac{eV}{T}$ and $\mu_{87} = (2.8164 \pm 0.0003) \times 10^{-5} \frac{eV}{T}$ respectively. A Rb absorption cross section measurement is preformed by monitoring the transmittance of a Rb cell as a function of the number density of gaseous Rb atoms. An application of the Beer-Lambert law gives $\sigma = (6.06 \pm 0.06) \times 10^{-17}$ m^2. We also note the power broadening of the resonance curves and explore the high magnetic field regime where the degeneracy of the z-component atomic angular moment quantum number M_F is broken.

INTRODUCTION

Rubidium (Rb) is an alkali metal with atomic number $Z = 37$. Neutral states contain four entirely filled electron shells with no net angular momentum and a single valence electron. In its ground state, the valence electron carries no orbital angular momentum: $5^2S_{1/2}$. In its first exited state, the valence electron carries one quanta of orbital angular momentum which can either align or anti-align with its spin contribution: $5^2P_{1/2}$ or $5^2P_{3/2}$.

The energy splitting of the 5^2S and 5^2P states due to the Coulomb interaction with the nucleus is on the order of a few electron-volts. The degeneracy of the first excited state is lifted by the spin-orbit coupling in which the electron's spin couples to the magnetic field set up by the positively charged nucleus in motion relative to the electron. This effect introduces an energy gap that is on the order of 10^{-2} electron-volts between the $5^2P_{1/2}$ and $5^2P_{3/2}$ states. A similar interaction between the nucleus and the magnetic field set up by the electron causes further energy splittings which are on the order of 10^{-9} electron-volts [1]. These energy levels are characterized by quantized z-component of the total, i.e. combined nuclear- and electron-, spin M_F which couple to the magnetic field oriented in the z-direction. It is this interaction that we will be probing by applying the techniques of optical pumping and magnetic resonance.

A Rubidium atom can transition between energy states by absorbing or emitting light. When a single photon is absorbed by an Rb atom, conservation of angular momentum imposes a selection rule that limits which states are accessible. By shining light of the appropriate energy onto a sample of Rb atoms, one can induce transitions from the ground state to the excited state. The helicity of the light determines determines whether the quantum number M_F will increase or decrease by one quanta per photon or remain constant. These excited states can relax by emitting a photon and re-excite by absorbing yet another photon. The relaxation process can increase, decrease, or not change M_F at random depending on the helicity of the emitted photon; however, controlling the helicity of the incident light dictates which way the atom can become excited. By continuing this process, all of the atoms in the sample will find themselves in either the maximal or minimal allowed M_F state. In this case, the sample is said to be *optically pumped* into that quantum state and is unable to absorb any more of the light due to the lack of an excited state allowed by the selection rule. [2]

By introducing an alternating magnetic field at a frequency corresponding to the hyperfine energy splitting, the Rb atoms are bathed in virtual photons with the correct energy to induce stimulated emission of real photons which relax the atom into a lower energy sublevel. No longer in the maximal/minimal allowed M_F state, the atom is not optically pumped and can once again absorb the incident light. By sweeping different frequencies and monitoring the intensity of the transmitted light through a sample, one can probe the energy splittings that are artifacts of the atomic structure's finer details.

REVIEW OF PREVIOUS WORK

In 1950, Alfred Kastler invented optical pumping to control the relative populations of Zeeman and Hyperfine levels in the ground state of atoms. This change in population was monitored by analyzing either transmitted light by the sample or scattered resonance light. This technique was also used to investigate excited states of atoms. The pioneering work in this direction was done by Brossel and Bitter in 1952, when they studied 6^3P_1 of the Mercury atom. [3]

Optical pumping was important for the study of light-matter interaction. It allowed the precision measurements of atomic energy levels, and it lead to other technological advancements, such as laser. The Nobel Prize in Physics 1966 was awarded to Alfred Kastler "*for the discovery and development of optical methods for studying Hertzian resonances in atoms.*" [4]

EXPERIMENTAL SET-UP

The schematic of experimental design is shown in figure 1. We use a Rubidium discharge lamp and a lens to produce collimated Rb D_1 and D_2 lines. We select circularly polarized D1 line by applying a spectral filter and a linear polarizer with a quarter wave plate. The filtered light is focused at a heated Rubidium Cell, which contains both ^{85}Rb and ^{87}Rb isotopes. The Rb cell also contains Argon (Ar) gas as a buffer. The light emerges from the cell is refocused at a Si photodiode, which converts light to current. The signal from the photodiode is amplified before recorded by LabView software.

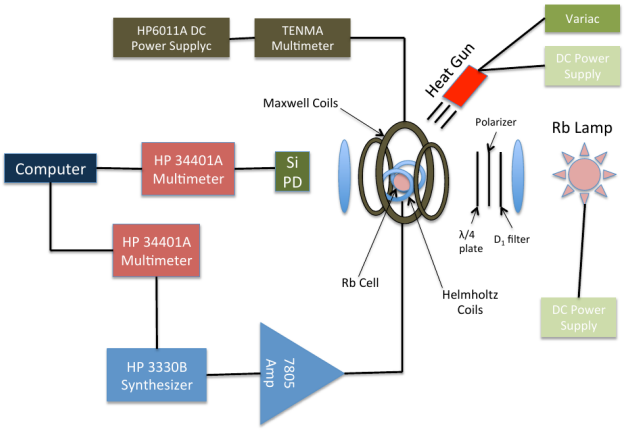

FIG. 1. Schematic of experimental setup

We use Maxwell coils to produce a uniform magnetic field around the Rb cell. The entire apparatus is titled, such that the center line of the apparatus is roughly parallel to the magnetic field of the Earth. The Maxwell coils are arranged into the three coil configuration originally designed by James Clark-Maxwell in 1873 [5]. This configuration enables us to convert DC current to a homogeneous magnetic field of known intensity. The Maxwell coils are consisted of two smaller coils (labeled A and C) and one larger coil (labeled B). Two smaller coils A and C are symmetrically placed with respect to coil B. The displacement between the center of coil B and the center of smaller coil is 26.5 ± 0.2cm.

The coils are wound with copper wire of known diameter, 0.132 ± 0.005cm. The inner diameter of coil B is 78.4 ± 0.5cm, while those of coil A and C are 59.1 ± 0.5cm [6]. The Maxwell coils are shown in Figure 2. A set of Helmholtz coils is placed orthogonal to the three Maxwell coils around the Rubidium cell. These second set of coils are used to generate Radio Frequency (RF) field, which is controlled by a synthesizer. We use the synthesizer to sweep a range of RF frequencies and locate the resonance peaks of ^{85}Rb and ^{87}Rb isotopes.

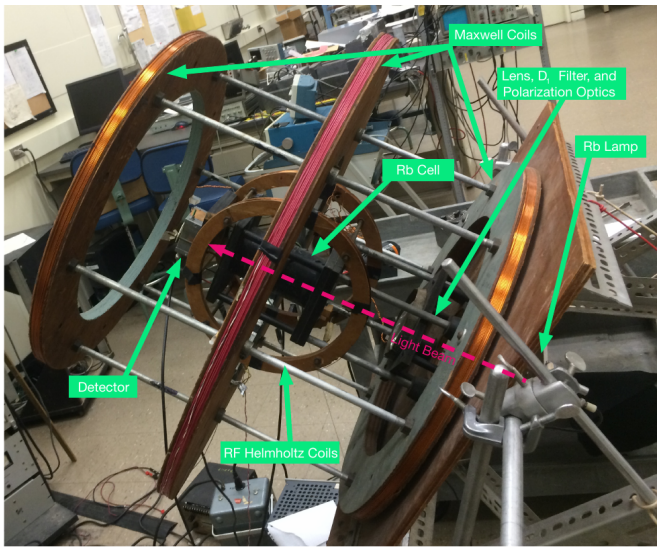

FIG. 2. The optical pumping experiment apparatus. The whole apparatus is tilted such that it is roughly aligned with the magnetic field of Earth. Rb cell is located at the center of the apparatus. Three bigger outer rings are Maxwell coils. Maxwell coils are labeled A, B, and C from left to right. Two smaller inner coils around Rb cell is Helmholtz coils used to generate radio frequency.

THEORETICAL MODEL

We first consider a atom with atomic number Z orbited by Z electrons. To the leading order, its energy levels are determined by Coulomb potential among the nucleus and electrons. Since the mass of the nucleus M is much greater than that of electron m_e, i.e. $M \gg m_e$, we use Born-Oppenheimer (BO) approximation to separate the motion of the nucleus and electrons. In the rest frame of the nucleus, the following Hamiltonian describes the leading order interaction

$$\hat{H}_0 = \sum_{n=i}^{Z} \left(\frac{-\hbar^2}{2m_e} \nabla_i^2 - \frac{1}{4\pi\epsilon_0} \frac{Ze^2}{r_i} \right) + \sum_{pairsij} \frac{1}{4\pi\epsilon_0} \frac{e^2}{|r_i - r_j|} \quad (1)$$

The first term is a electron kinetic term. The second and third terms describe Coulomb interaction between the nucleus and a electron and among electrons respectively. In general, the third term is nonlinear and there is no analytic solution to this Hamiltonian. Hydrogen like atom, which one studies in a elementary quantum mechanics course, is such special case. For a Hydrogen like atom, the solution to Equation 1 and the corresponding energy levels are given by.

$$\psi_{nlm}(r, \theta, \phi) = R_{nl}(r) Y_l^m(\theta, \phi) \quad (2)$$

$$E_n = \frac{-m_e c^2 \alpha^2 Z^2}{2n^2} \quad (3)$$

where α is the fine structure constant, and n, l, and m are quantum numbers described below. To the leading order, the energy level of a Hydrogen like atom is solely determined

by its radial quantum number n. The other two quantum numbers l and m determine electron orbital momentum and the z component of electron orbital momentum respectively.

We can use the solution and energy levels as a framework to describe more complex atoms like Rb. The Pauli Exclusion principle forbids two identical fermions from occupying the same quantum state. This allows us to"build up" a multi-electron solution by filling the lowest energy levels before filling the higher levels. This idea is summarized in the Aufbau principle.

In this experiment, we use RB atoms which have 37 electrons. Its full ground state configuration is $1s^2 2s^2 2p^6 3s^2 3p^6 3d^{10} 4s^2 4p^6 5s^1$. Because the core electrons are "invisible" to our spectroscope, we can simplify our analysis by only considering single valence electron in $n = 5$ state.

In the previous model, which only considers Coulomb interaction, energy levels are insensitive to electron spin, nuclear spin, and the z-component of the total angular momentum. Each of them results in energy level degeneracy. In order to break this, we need to make a series of relativistic corrections to our Hamiltonian equation $\hat{H}_0$. In the weak magnetic field limit, under which this experiment is performed, they are spin-orbit coupling, hyperfine splitting, and Zeeman effect, listed from largest to smallest effect.

Spin-orbit coupling for ^{87}Rb is shown in Figure 3. Spin-orbit coupling is due to the interaction between the spin of a electron and the magnetic field generated by a nucleus moving relative to it. Depending on whether the electron spin "anti-aligns" with orbital angular momentum, energy levels either shift up or down. In this experiment, spin-orbit coupling breaks $5P$ energy level degeneracy. The energy of spin "aligned" state $5^2P_{1/2}$ is lowered, while that of "anti-aligned" state $5^2P_{3/2}$ is raised. Spin-orbit coupling is about 9 orders of magnitude smaller than Coulomb interaction. For Rubidium, the effect is about 0.03 eV [1].

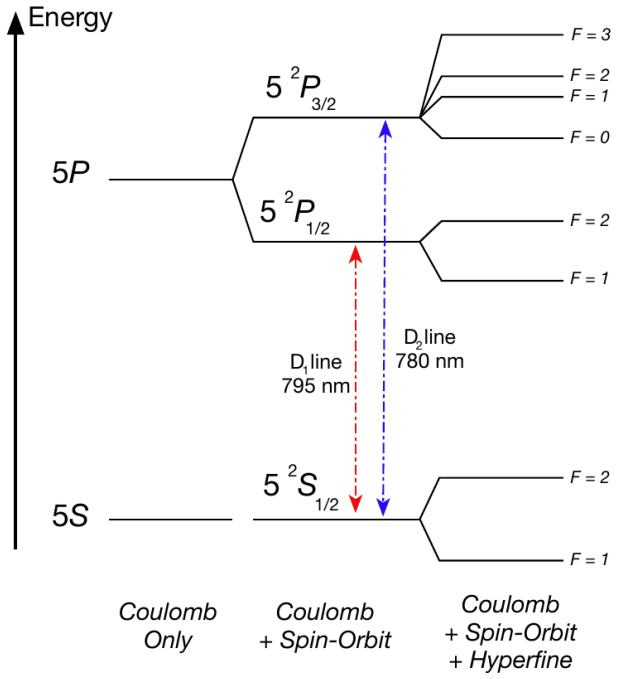

FIG. 3. Schematic diagram of ^{87}Rb energy levels. In the first column, the ground state energy levels of the Coulomb only model is shown. The change of energy levels due to relativistic corrections, spin-orbit coupling and hyperfine splitting, are shown in the column 2 and 3 respectively. Note that the total angular momentum quantum number F is used to label the last column.

Hyperfine Splitting

The next order correction to our Hamiltonian is hyperfine splitting, which is due to the interaction of nuclear spin and the magnetic field produced by electrons. In general, the interaction between a spin and magnetic field modifies Hamiltonian by

$$\hat{H} = -\mu \cdot B \tag{4}$$

In the case of hyperfine splitting, the relevant magnetic moment is the magnetic moment of nucleus μ_I and the magnetic field B_e produced by electrons. For a nucleus with spin angular momentum I, its magnetic moment is given by the Equation $\mu_I = g_I \mu_N I$. Here μ_N is the nuclear magneton and g_I are the nuclear landau g-factor.

Hyperfine splitting is described by a set of four quantum numbers, J, I, F, and M_F. The total electron angular momentum number J and nuclear spin number I, along with the total angular momentum number $F = J + I$ and the z-component of the total angular momentum number M_F. Hyperfine energy levels are sensitive to the total angular momentum F. The hyperfine splitting of ^{87}Rb is shown in Figure 3. In this experiment, the hyperfine splitting is about 10 neV [1], which is about 6 orders of magnitude smaller than the spin-orbit effect.

Zeeman Effect

We have lifted the energy level degeneracies by including the interaction between spins, electron and nuclear, with the internal magnetic fields. It remains to break the degeneracy due to the spherical symmetry of atom. In the absence of a external field, a atom does not have a preferred direction, and its energy levels do not depend on a directionally dependent quantity. In particular, the hyperfine energy levels, shown in Figure 3, are insensitive to the z component of the total angular momentum. This leaves each hyperfine energy level $2F + 1$ folds degenerate. Zeeman effect is the breaking of this degeneracy by applying an external magnetic field. In the weak field limit, Zeeman effect modifies our Hamiltonian by

$$\hat{H}_{zeeman} = -g_F \frac{\mu_B B_{ext}}{\hbar} \hat{F}_z \tag{5}$$

where g_F is the hyperfine landau g-factor. Zeeman effect of ^{87}Rb is shown in Figure 4.

In the strong B field limit, Zeeman effect is replaced with Paschen-Back effect. The physics behind both effects are the same. However, the Paschen-Back effect is larger than hyperfine splitting in this regime, and the good quantum numbers become j,l,s and i. Paschen-Back Hamiltonian is given by

$$\hat{H}_{PB} = -\frac{\mu_B B_{ext}}{\hbar}(g_J \hat{J}_z + g_I \hat{I}_z) \tag{6}$$

where g_J and g_I are the total electron and nuclear landau

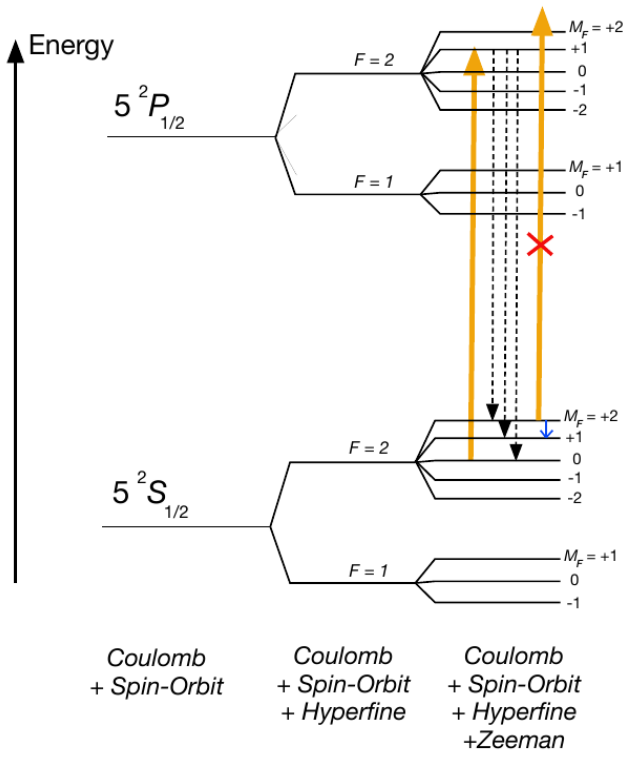

FIG. 4. Schematic diagram of ^{87}Rb optical pumping process. When ^{87}Rb atoms in ground state absorb σ^+ photons, excitation processes must satisfy $\Delta M_F = +1$ (the left yellow arrow). When excited atoms relax, available transitions are $\Delta M_F = \pm 1$ or $\Delta M_F = 0$, depending on the helicity of emitted photon. (the three dashed arrows). Selection rule forbids atoms in the $M_F = +2$ ground state from being excited. (the right yellow line)

g-factors. In the intermediate regime, the solution is a linear combination of the weak field solution and the strong field solution.

Optical Pumping and Magnetic Resonance

A atom can transition between energy states by absorbing or emitting a photon. The conservation of angular momentum imposes a selection rule, which constrains the possible transitions between quantum states. The following lists describe the selection rule for a single photon transition.

- Absorption: The total angular momentum increases by one quanta. The z-component of the total angular momentum either increases, decreases, or stay constant, depending on the helicity of the absorbed photon.
- Emission: The total angular momentum decreases by one quanta. The z-component of the total angular momentum either increases, decreases, or stay constant, depending on the helicity of the emitted photon.

In this experiment, we use Rb D1 light to excite Rb atom from S state to P state. Without the loss of the generality, we focus on the case where the absorbed photon has σ^+ helicity. As shown in Figure 4, the ground state with $M_F = 2$ does not have an allowed exited states. So once a Rubidium atom enters this state, it remains there. As the excitation and relaxation process continue, more and more Rb atoms enters into the state. Eventually, all Rb atoms are optically pumped into the state.

An alternating magnetic field at a frequency corresponding to the magnetic resonance frequency can cause a spontaneous emission of a photon. A Rubidium atom that goes through this process is no longer in the optically pumped state and can be excited again. In this experiment, we determine the magnetic resonance frequency by measuring this re-absorption signature.

MEASUREMENTS

The optical pumping and magnetic resonance technique allows for a rich suite of measurements to probe the detailed atomic structure of relatively complicated elements. Here we present measurements of the absorption cross-section of (optically pumped) Rubidium gas, the magnetic moments of the ^{85}Rb and ^{87}Rb isotopes, power broadening of the ^{85}Rb resonance peak, and hyperfine splitting.

Rb Absorption Cross Section

The absorption cross section of Rubidium was measured as the Rb cell warmed through the application of the Beer-Lambert law, which predicts the following relationship between the transmitted intensity of light and the number density of Rb atoms [7]:

$$I = I_0 e^{-\sigma n l}. \tag{7}$$

Here I is the transmitted intensity, I_0 is the intensity of the incident light, σ is the absorption cross section, n is the number density of Rb atoms, and $l = 0.05$ m is the cell length. The transmittance for a given Rb density was recorded via the photodiode, and the temperature of the cell was measured crudely with a mercury thermometer for each reading. The monatomic Rubidium gas inside the cell is well-described by the ideal gas law

$$n = \frac{N}{V} = \frac{P(T)}{k_b T}. \tag{8}$$

At constant volume, the pressure of Rubidium gas as a function of temperature has been parameterized as the following:

$$P(T) = 10^{4.857 - 4215/T} \text{ atm} \tag{9}$$

where temperature T is given in units of Kelvin. Putting together Equations 8 and 9 allows the determination of the Rb number density from the temperature measurements:

$$n(T) = \left(\frac{101325.0 \text{ Pa}}{1 \text{ atm}}\right) \frac{(10^{4.857-4215/T} \text{ atm})}{(1.38 \times 10^{-23} \text{J/K}) T} \tag{10}$$

$$= 1.006 \times 10^{33} \left(\frac{10^{-4214/T}}{T}\right) \text{ m}^{-3} \tag{11}$$

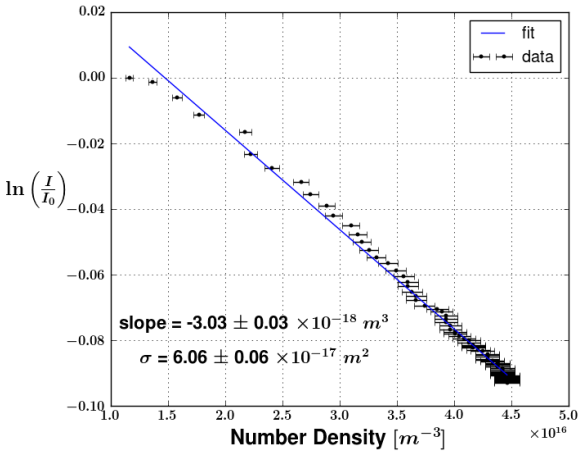

FIG. 5. The absorption cross section of Rubidium from the application of Beer-Lamberts law to data taken as the Rb cell warmed.

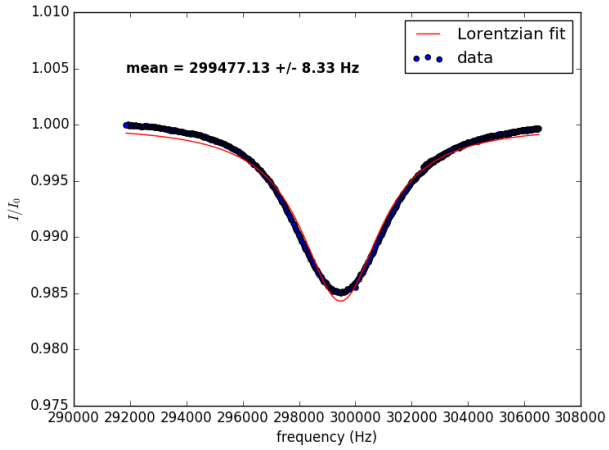

FIG. 6. A typical resonance curve shows a characteristic dip in intensity of transmitted light, indicating the alternating magnetic field in which the Rb sample is immersed is on resonance with the hyperfine energy splitting.

Figure 5 shows the data from which the cross-section was calculated to be

$$\sigma = (6.06 \pm 0.06) \times 10^{-17}\ \mathrm{m}^2. \tag{12}$$

The uncertainty in the samples temperature, σ_T, is responsible for that of the number density for the data in Figure 5. A mercury thermometer was inserted into the sample which allowed for crude temperature readings. We estimate $\sigma_T = 0.25$ K. The error is propagated according to Equation 11.

^{85}Rb and ^{87}Rb Magnetic Moment

When the sample is in an optically pumped state, it is unable to absorb the 795 nm D1 light from the heat lamp. Consequently all of the light is transmitted and detected by the photodiode. As the frequency of the alternating magnetic field set up by the Helmholtz coils approaches magnetic resonance, the atoms begin to drop from their optically pumped states and are thus able to absorb the D1 light. In this case, the amount of transmitted light and therefore the photodiode reading will drop. See Figure 6 for an example of such a resonance curve. By sweeping over a band of frequencies, one can deduce the energy splittings of the hyperfine structure by identifying the frequency which causes a drop in the photodiode signal and converting it to energy via

$$E = h\nu. \tag{13}$$

See Figure 6 for an example of a typical resonance curve.

The magnitude of this energy splitting is given by Equation 4, which illustrates its linear dependence on the on the magnetic field present. The proportionality factory, the nuclear magnetic moment μ_I was measured for both isotopes of Rb by varying the DC magnetic field with the Maxwell coils and finding the associated energy splitting. Data from this procedure are shown in Figure 7.

The error of the energy splitting for each data point was estimated by repeating the measurement 20 times for both

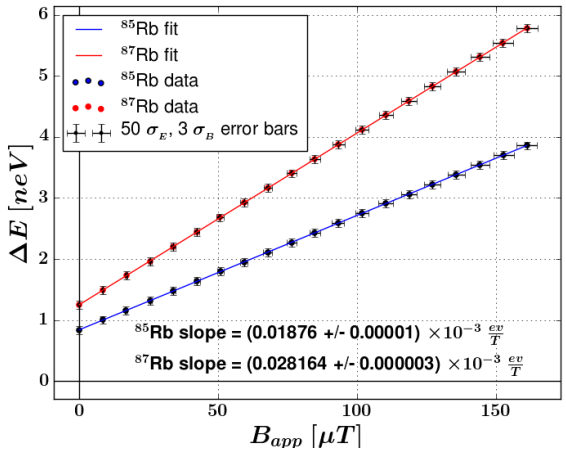

FIG. 7. Hyperfine energy splitting as a function of the applied magnetic field. The slope of the linear relationship give the magnetic moments magnetic moments of the ^{85}Rb and ^{87}Rb isotopes.

no applied magnetic field and the maximum applied magnetic field of about 161 μT and calculating the variance. This showed that the absolute error, not the relative error, is what scales with the energy splitting and was determined to be $\sigma_{\Delta E} = 0.0013$ neV (stat). The error in the applied magnetic field arises from contributions from the uncertainties in the dimensions and positioning of the Maxwell coils as well as that of the current pushed through the coils. σ_B is field dependent and on the order of 1%.

Ambient Magnetic Field

In the absence of an applied magnetic field as supplied by the Maxwell coils, there is an ambient field present due to the Earth's magnetic field, the atomic magnetic field, and any residual magnetic field from the laboratory equipment surrounding the experimental setup. A measurement of this ambient field was performed by considering the energy splitting for no applied magnetic field in Figure 7.

Applying Equation 5 to the measured energy splittings of ^{85}Rb and ^{87}Rb under no applied field, the magnitude of the ambient field is found to be

$$B_{ambient} = 42.717 \pm 0.075\,\mu T \tag{14}$$

and

$$B_{ambient} = 42.610 \pm 0.093\,\mu T, \tag{15}$$

respectively.

The reported uncertainties are statistical in nature and are estimated by repeating the resonance sweep 20 times. These measurements are consistent with one another and of the same order of magnitude as the magnetic field due to Earth at Stony Brook University, $B_{Earth} = 51.704\,\mu T$ [8], suggesting this is the main contribution to the ambient field.

Power Broadening

Power broadening refers to the phenomena in which the width of a spectral resonance curve increases with the power of the incident light. The incident light is responsible for inducing both the stimulated absorption and stimulated emission of the Rb atomic states. The rate of stimulated emission is proportional to the number of excited states, while stimulated absorption is more strongly correlated with the intensity of the beam [9]. As the intensity of the light increases, its tendency to stimulate emission exceeds its tendency to stimulate absorption. As a consequence, the range of frequencies that noticeably demonstrate a dominance of stimulated absorption over emission increases with beam intensity.

High Field Regime

With a sufficiently high magnetic field, the magnetic resonance curves are sensitive to the particular M_F quantum number of a given atomic state in addition to the change in M_F from a transition. In this field regime, one can observe multiple resonance peaks for a given isotope. Figure 9 is an example of the hyperfine splitting of ^{85}Rb under the presence of an applied 413 μT field.

The height of each peak is proportional to the differential occupation number, i.e. the difference between the occupation number of the initial and final states. Figure 9 shows that the state corresponding to the lowest energy shift is most populated. Furthermore, the non-linear behavior of the Breit-Rabi formula in the high-field regime predicts the energy spacing between two high M_F states will be lower than that of two low M_F states [10]. It follows that the optically pumped state in this experiment was the $F = 2$ $M_F = +2$ state. Clearly, the linear polarizer and quarter wave plate were set up to allow the right handed circular light (σ_+) to impinge the Rb cell.

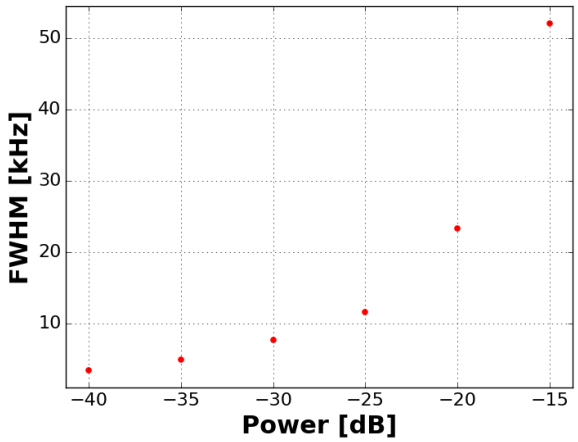

FIG. 8. Power broadening of the ^{85}Rb resonance peak. The full width at half max (FWHM) of the resonance curve as a function of the synthesizer amplitude feeding the Helmholtz coil.

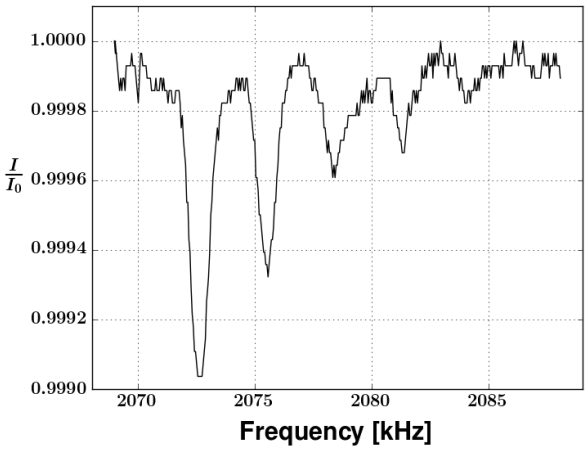

FIG. 9. (data) Observation of hyperfine splitting of ^{85}Rb.

DISCUSSION AND CONCLUSIONS

By optically pumping a sample of ^{85}Rb and ^{87}Rb and monitoring its transmittance while experience a range of alternating magnetic field frequencies, the hyperfine atomic structure was probed. The absorption cross section of Rb was measured to be $\sigma = (6.06 \pm 0.06) \times 10^{-17}$ m^2 while preparing the experimental conditions. To measure the magnetic moment of both Rb isotopes, the hyperfine energy splitting dependence on the applied external magnetic field was measured. The astonishingly linear relationship is a testament to the precision this technique has to offer; the linear fit gives a slope error of 0.05%. Figure 7 shows

$$\mu_{85} = (1.876 \pm 0.001) \times 10^{-5}\,\frac{eV}{T} \tag{16}$$

and

$$\mu_{87} = (2.8164 \pm 0.0003) \times 10^{-5}\,\frac{eV}{T}. \tag{17}$$

The data in Figure 7 also gives independent measurements of the ambient magnetic field (Equations 14 and 15) which are consistent within 1σ. Exploring this technique also demonstrated the phenomena of power broadening, shown in Figure 8.

Perhaps the most impressive feature of optical pumping and magnetic resonance is its ability to measure energy splittings that are billions of times smaller than the Coulomb interaction, which is the dominating influence in the atomic structure. This study has demonstrated how this very straightforward method and practically feasible setup can explore atomic structure on the nano-electron-volt scale with a very high degree of precision.

AUTHOR CONTRIBUTIONS

Both authors contributed to the data acquisition and analysis; however, the former was led by D. Han and latter by K. Wood.

D. Han wrote the "Experimental Set-Up", "Theoretical Model", and "Review of Previous Work" sections, while K. Wood wrote the "Abstract", "Introduction", "Measurements", and "Discussion and Conclusions" sections.

[1] T.K. Allison, PHY 445/515 Optical Pumping and Magnetic Resonance. Stony Brook University, 2015

[2] W. Happer, Rev. Mod. Phys. **44**, 169 (1972)

[3] C. Cohen-Tannoudji and A. Kastler (1996) pp. 1-81

[4] Nobel Media, "The Nobel Prize in Physics 1966"

[5] J. C. Maxwell, *Treatise on Electricity and Magnetism, Vol. 1* (Dover Publications, 1954)

[6] Advanced Laboratory Lab Manual: Optical Pumping , Stony Brook University, 2002

[7] P. Siddons, C. Adams, C. Ge, and I. Hughes, arXiv:0805.1139

[8] `https://www.ngdc.noaa.gov/geomag-web/#igrfwmm`

[9] Levine, Jonathan. "A Simplified Calculation Of Power-Broadened Linewidths, With Application To Resonance Ionization Mass Spectrometry". *Spectrochimica Acta Part B: Atomic Spectroscopy* 69 (2012): 61-66. Web.

[10] `http://home.sandiego.edu/~severn/p480w/OP_TW_5.pdf`

Appendix

The full experimental dataset and corresponding analysis tools used in this paper are available at `https://github.com/dwhan89/SBU_P515`.